ments for the Chemical Engineering degree at the University of Palermo, March 1981.

Manuscript submitted June 21, 1983; revised manuscript received Aug. 1, 1984.

The Universita di Palermo assisted in meeting the publication costs of this article.

REFERENCES

1. A. Güntherschultze, *Phys. Z.*, **24**, 212 (1923).
2. H. Frölich, *Rpt. Prog. Phys.*, **6**, 143, (1939), and references therein.
3. F. Forlani and N. Minnaja, *Phys. Status Solidi*, **4**, 311 (1964).
4. J. J. O'Dwyer, *This Journal*, **116**, 239 (1969).
5. D. A. Vermilyea, *ibid.*, **110**, 345 (1963).
6. R. S. Alwitt, A. J. Breen, and J. S. L. Leach, in "Oxide-Electrolyte Interfaces," R. S. Alwitt, Editor, p. 265, The Electrochemical Society Softbound Proceedings Series, Princeton, NJ (1973).
7. S. F. Bubar and D. A. Vermilyea, *This Journal*, **113**, 892 (1966).
8. L. C. Archibald and J. S. L. Leach, *Electrochim. Acta*, **22**, 15 (1977).
9. L. C. Archibald and J. S. L. Leach, *ibid.*, **22**, 21 (1977).
10. V. R. Howes, *Corros. Sci.*, **14**, 491 (1974).
11. D. H. Bradhurst and J. S. L. Leach, *This Journal*, **113**, 1245 (1966); *ibid.*, **113**, 1284 (1966).
12. J. S. L. Leach and B. R. Pearson, in "Proceedings of the 7th International Congress on Metallic Corrosion," p. 151, Rio de Janeiro (1978).
13. N. Sato, *Electrochim. Acta*, **16**, 1683 (1971).
14. J. Yahalom and J. Zahavi, *ibid.*, **16**, 603 (1971).
15. J. Yahalom, in "Oxide-Electrolyte Interfaces," R. S. Alwitt, Editor, p. 288, The Electrochemical Society Softbound Proceedings Series, Princeton, NJ (1973).
16. A. K. Vijh, *Corros. Sci.*, **11**, 411 (1971).
17. S. Ikonopisov, *Electrochim. Acta*, **22**, 1077 (1977).
18. S. G. Christov, *J. Electroanal. Chem.*, **105**, 275 (1979).
19. F. Di Quarto, S. Piazza, and C. Sunseri, *This Journal*, **130**, 1014 (1983).
20. B. Cox, *ibid.*, **117**, 654 (1970).
21. S. Ikonopisov, A. Girginov, and M. Machkova, *Electrochim. Acta*, **24**, 451 (1979).
22. A. Güntherschultze and H. Betz, "Electrolyt-Kondensatoren," pp. 116-122, Technischer Verlag Herbert Cram, Berlin (1952).
23. G. C. Wood and C. Pearson, *Corros. Sci.*, **7**, 119 (1967).
24. F. J. Burger and J. C. Wu, *This Journal*, **118**, 2039 (1971).
25. N. Cabrera and N. F. Mott, *Rpt. Prog. Phys.*, **12**, 163 (1949).
26. A. T. Fromhold, Jr., *This Journal*, **124**, 538 (1977).
27. G. T. Rogers, P. H. G. Draper, and S. S. Wood, *Electrochim. Acta*, **13**, 251 (1968).
28. J. C. Banter, *This Journal*, **114**, 508 (1967).
29. N. Baba, *J. Less-Common Met.*, **43**, 295 (1975).
30. J. A. Davies, B. Domeij, J. P. S. Pringle, and F. Brown, *This Journal*, **112**, 675 (1965).
31. R. Piontelli, in "Symposium Proceedings on Sulphamic Acid and its Electrometallurgical Applications," Milan, May 1966, pp. 175, 437, Associaz. Ital, Metall., Milano (1966); L. Peraldo Bicelli, *ibid.*, pp. 19-27.
32. L. Young, *Trans. Faraday Soc.*, **55**, 632 (1959).
33. F. Di Quarto, A. Di Paola, and C. Sunseri, *This Journal*, **127**, 1016 (1980).
34. J. J. Randall, W. J. Bernard, and R. R. Wilkinson, *Electrochim. Acta*, **10**, 183 (1965).

Plasma Etching of Oxygen Containing Titanium Silicide Films

F.Y. Robb*

Motorola, Incorporated, Process Technology Laboratory, SRDL, Phoenix, Arizona 85008

ABSTRACT

Anisotropic etching of titanium silicide is essential if its low resistivity gate properties are to be utilized on scaled MOS devices. CCl_4 and CF_4 plasmas, as well as ion milling, were used to etch composite titanium silicide/polysilicon films, with each displaying definite drawbacks. CCl_4 plasmas yielded rough etching and etch residue, presumably due to the high oxygen content of the silicide film and the relatively high selectivity (low oxide etch rate) of the etch. CF_4 reactive ion etching and ion milling produced smooth etching but lacked the selectivity to stop on thin underlying gate oxides. A combination of these processes, however, provided successful anisotropic patterning of such structures. A nonselective, smooth etching CF_4 reactive ion etch was used to etch through the silicide layer, followed by a higher selectivity Cl_2 plasma etch through the underlying polysilicon down to the thin gate oxide.

Anisotropic etching of titanium silicide is essential if its low resistivity is to be utilized on scaled MOS devices.

Increases in packing density and complexity of MOS devices have increased the importance of the interconnect technology (1, 2). With the sheet resistance of even the most heavily doped polysilicon greater than 15 Ω/□, the advantages of further scaling will soon be offset by the interconnect resistance at the gate level. The selection of a lower resistivity gate material, together with the shortening of interconnect lengths by circuit designers, is essential in order to take advantage of the higher switching speeds of scaled down devices.

The low resistivity refractory metal silicides, with sheet resistances over an order of magnitude lower than polysilicon (3, 4), offer an attractive alternative. Replacing polysilicon entirely with the silicide, however, entails major changes in device design and processing and, perhaps most importantly, introduces an interface at the gate oxide of questionable stability. Thus, the more conservative approach has been to replace enough of the doped polysilicon with the silicide to achieve the desired resistance goal, but not so much as to cause a change in the effective metal-semiconductor work function (and thereby gate threshold voltage).

* Electrochemical Society Active Member.

Since titanium silicide ($TiSi_2$) has one of the lowest resistivities of the refractory metal silicides, very low resistivity titanium polycide gates can be achieved. In fact, a titanium polycide structure of 1500Å of silicide over 1500Å of polysilicon has a composite resistance of 1 to 2 Ω/□ (5), more than an order of magnitude lower than straight doped polysilicon.

The etchability of titanium silicide is, of course, one of the prime processing considerations. Anisotropic etching is essential in order to produce the fine patterns required for scaled MOS devices.

Little information is available on the etching of titanium silicide. Wang *et al.* (6) have reported the successful use of chlorine plasma etching for the patterning of composite $TiSi_2$/polysilicon gate structures, but found an extreme sensitivity to contamination in the film and required that the oxygen level in the film be less than 0.5%. In practice, obtaining such a low oxygen content in titanium silicide films is difficult and perhaps unnecessary, as resistances as low as 1 Ω/□ have been obtained on films containing 5% oxygen (5).

Downloaded on 2016-02-18 to IP 130.203.136.75 address. Redistribution subject to ECS terms of use (see ecsdl.org/site/terms_use) unless CC License in place (see abstract).

GF Exhibit 1053 - 1/6

The plasma-etch characteristics of oxygen containing titanium silicide films is the subject of the present study. CCl_4 and CF_4 reactive ion etching, as well as ion milling, will be detailed and contrasted. Successful anisotropic etching could not be accomplished in any one-step etch; it required two etch steps. The first step used a low silicon-to-oxide etch-rate ratio to etch smoothly through the oxygen containing silicide. The second step, in contrast, utilized a high silicon-to-oxide etch-rate ratio to pattern the underlying polysilicon and stop on the thin gate oxide.

Experimental

Etch systems.—Several different etch systems were used in this study.

CCl_4 plasma etching was studied in a single-wafer planar reactor. The top electrode was powered (13.56 MHz), while the etching wafer was placed on the lower grounded electrode. An upper-to-lower electrode-area ratio of 2 to 1 was utilized. All surfaces exposed to the plasma were passivated with an anodized aluminum coating. Wafer cooling was provided by a cold (10°C) plate physically affixed to the lower electrode. A gas mixture of 8 sccm CCl_4, 7 sccm Ar, 8 sccm N_2, and 3 sccm H_2, at 300 μm with 1 W/cm^2 was used. This process was developed for anisotropic etching of N^+ polysilicon.

CF_4 etching was performed in two reactors.

Initial CF_4 studies utilized a laboratory-scale diode configured reactor. The wafers were positioned on the smaller powered (13.56 MHz) electrode, while the outer chamber walls acted as the grounded anode. The chilled (10°C) cathode, which held nine 3 in. substrates, was covered with a thin silicon plate to minimize metallic contamination. A flow rate of 7 sccm CF_4, with a 100 μm pressure, and 0.55 W/cm^2 was used.

The temperature dependence of CF_4 etching was measured in a Perkin-Elmer Omni-Etch Cornerstone single-wafer etcher, where the wafers were physically clamped to a temperature-controlled lower electrode. The system had a powered (200 kHz) porous graphite top electrode. A flow rate of 50 sccm CF_4, with a 800 μm pressure, and 1.5 W/cm^2 was used.

The Cornerstone was also used for low frequency Cl_2 plasma etching of polysilicon in the second step of the two-step polycide etch process. Process conditions used were 100 sccm Cl_2, 800 μm pressure, 0.7 W/cm^2, and a 5°C lower electrode. No undercutting of even highly doped N^+ polysilicon was observed.

All plasma-etch systems used standard rotary pumps and maintained base pressures of between 20 and 40 μm. Mass flowmeters were used to monitor gas flow and pressure was measured with capacitance manometers.

Ion milling was performed in the Veeco Microetch system, which utilized a 10 in. diffusion pump and a Kaufman-type ion gun. Typical milling conditions were 0.4 mA/cm^2, 600V, and 9.0×10^{-4} torr argon pressure. Milling angles between 0° and 15° were studied.

Sample preparation and analysis.—Titanium silicide films were cosputtered in a Sputtered Films, Incorporated, Research System with a Ti:Si ratio of 1:2.2. At this composition, the resistivity after anneal was about 17 $\mu\Omega \cdot$ cm.

Auger electron spectroscopy (AES), in conjunction with sputter profiling, was used to analyze the samples as a function of depth. As shown in Fig. 1, deposited films were uniform, incorporated an atomic oxygen concentration of about 5%, and had a native oxide thickness of between 50 and 100Å. After anneal, the bulk oxygen content decreased slightly, as apparently some of the oxygen diffused to the surface to react with Ti or Si. The surface oxide thickness after anneal was about twice that of the nonannealed films.

Unannealed pure titanium films, sputter-deposited in the same system, were etched for comparison. AES profiling showed a similar oxygen content and native oxide as for the unannealed silicide.

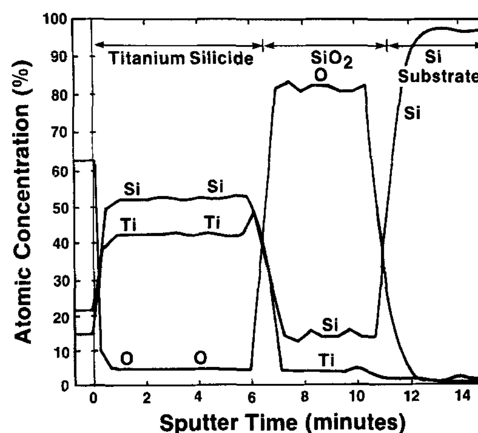

Fig. 1. Auger depth profile of an as-deposited $TiSi_{2.2}$ film. This film was deposited directly on thermal oxide.

The $TiSi_2$ film was typically 1500-2000Å thick and deposited directly on a 2000Å thick polysilicon film. Underlying the polysilicon was gate oxide. The polysilicon was phosphorus doped via either standard ion-implantation techniques or by 950°C PH_3 diffusions. In most cases, no annealing of the $TiSi_2$/poly was done prior to etch, although where specified a 950°C, 30 min N_2/H_2 anneal was utilized. On these samples, a 1000Å CVD oxide cap was deposited on top of the silicide to stop out-diffusion of phosphorus from the underlying polysilicon. The cap was removed via CHF_3 reactive ion etching after photoresist masking but before subsequent polycide etching.

KTI II and AZ-1350J positive photoresists, as well as trilevel (7, 8) plasma oxide/HPR-204 masks, were used to produce patterned samples.

Analytical techniques.—Silicide and resist rates were calculated from etch depth measurements made on the Tencor 10-0020 Alpha Step. Polysilicon and oxide rates were calculated from thickness measurements made on an IBM 7840 Film Thickness Analyzer.

The surface roughness as a function of the etch technique was quantified with reflectance data from the IBM 7840. The reflectance of each sample was measured and plotted as a function of wavelength from 4300 to 7000Å. In order to simplify data reporting, an "average" reflectivity was calculated from the maximum and minimum reflectances, as shown below

$$R = \frac{R_{max} + R_{min}}{2}$$

All reflectivities are reported as a percentage of an evaporated aluminum standard measured at the same time.

Cross-sectional scanning electron micrographs (SEM's) of patterned samples were utilized to determine etch anisotropy.

AES was used to analyze the cleanliness of etched surfaces.

Results and Discussion

CCl_4 etching.—Table I summarizes the etch data from the single-wafer etcher. The unannealed silicide etched at about the same rate as polysilicon, whereas the annealed silicide etched about 20% more slowly. In addition, the pure titanium etch rate was considerably higher than that of either polysilicon or the silicide. The fast titanium rate was unexpected, considering the reported volatilities of the expected etch products. $SiCl_4$, the more volatile product, has a vapor pressure of 1 torr at −63.4°C, while $TiCl_4$ has a similar vapor pressure at −13.9°C (9).

A simple evaporation model allows an estimate of the maximum $TiSi_2$ etch rate achievable from evaporation only. The model assumes thermal equilibrium, so that the number of molecules condensing must equal the number evaporating. From simple kinetic theory, the number condensing is assumed to be 1/4 $n\bar{v}$, where n is the num-

Downloaded on 2016-02-18 to IP 130.203.136.75 address. Redistribution subject to ECS terms of use (see ecsdl.org/site/terms_use) unless CC License in place (see abstract).

Table I. CCl_4 plasma etch data from the single-wafer etcher with 8 sccm CCl_4, 7 sccm argon, 8 sccm N_2, and 3 sccm H_2, a 300 μm pressure and 1 W/cm^2

Film	Etch rate (Å/min)	Etch residue	Anisotropy* (with resist mask)
Titanium silicide			
Unannealed	2300	Dense	Good
Annealed	1800	Moderate	Good
Polysilicon	2200	None	Excellent (undoped) Good (N^+ poly)
Titanium	3400	Dense	Good
Thermal SiO_2	350	—	—
Positive resist	800	—	—

* "Excellent" means zero undercut with 50% overetch. "Good" means zero undercut with 10% overetch and slight notching with 50% overetch. "Fair" means very slight undercut with 10% overetch.

ber of molecules per cubic centimeter and $\bar{v}$ is the average molecular speed. Using this model and the above vapor-pressure data, a maximum $TiSi_2$ etch rate of 10^7 Å/ min is calculated. The poor agreement with the measured etch rate of 2300 Å/min indicates that evaporation is not the rate-limiting step of the etch mechanism.

Figure 2 shows composite titanium silicide/polysilicon films etched in the CCl_4 process. The anisotropy of the CCl_4 etch was good, with no undercutting observed for a 10% overetch and only very slight notching with a 50% overetch. Etch residue, however, plagued the etch. The residue was presumed to be simply unetched polysilicon, since Auger analysis of etched surfaces found only silicon, oxygen, and carbon. Because N^+ poly was used for the polycide gate, the residue provided conductive paths and was therefore unacceptable. Although longer overetches somewhat reduced the residue height and density, the thin underlying gate oxide prohibited this.

The etch residue was attributed to rough etching of the $TiSi_2$ layer. Reflectivity, which provides a quantitative measure of the roughness is plotted as a function of etch depth in Fig. 3. Within experimental error, no differences can be seen between the unannealed silicide and pure titanium films. Both became extremely rough as etching proceeded. This roughness, which was then replicated into the underlying polysilicon layer, resulted in the etch residue. The annealed silicide, surprisingly, etched much more smoothly. In addition, the reflectivity of virgin polysilicon as a function of depth is also plotted for comparison and shows that polysilicon films by themselves etched quite smoothly.

The rough etching was attributed to both the presence of a native oxide and to the relatively high oxygen content of titanium containing films. Auger analysis revealed that all the titanium containing films had more than an order of magnitude more oxygen than polysilicon. In addition, although the thickness of the native oxide on both polysilicon and unannealed $TiSi_2$ films was comparable (50Å), the oxide on the silicide contained titanium. The "toughness" of titanium oxide is well known to ion millers (10), as it is reported to have one of the lowest known milling rates.

The relatively low oxide etch rate of the CCl_4 process meant submicron sized "oxide" inclusions in/on the film would act as micromasks, blocking etching of the underlying material. Rough etching, and ultimately etch residue, would result.

The role of the bulk *vs.* surface oxide was separated by comparing the two samples shown in Fig. 2. The annealed sample, which was given a CHF_3 pre-etch to remove its CVD oxide cap (and would also remove any native oxide), showed a much cleaner etched surface than the unannealed sample. A similar CHF_3 pre-etch of unannealed films also produced cleaner etching. Since both films still yielded etch residues even after native ox-

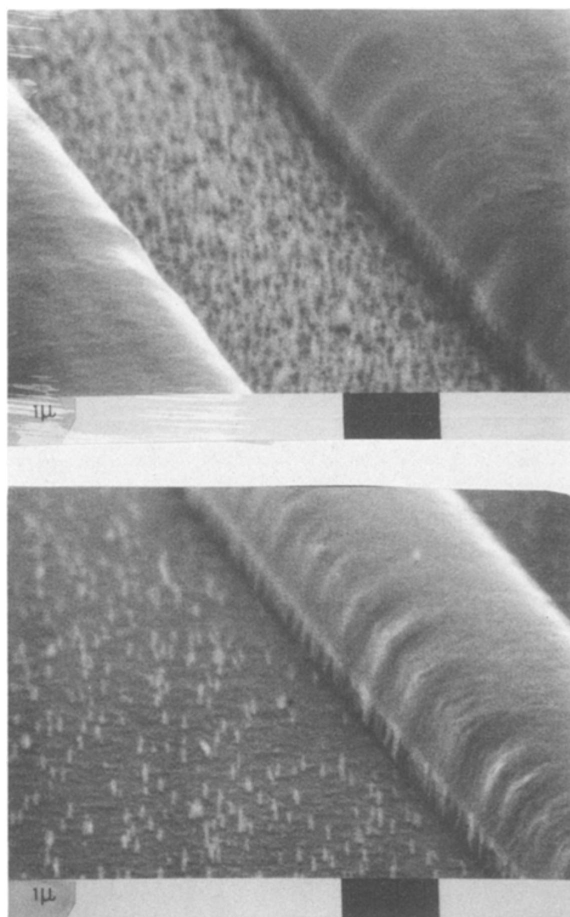

Fig. 2. Composite 2 kÅ titanium silicide/2 kÅ polysilicon films etched in the CCl_4 process. The bottom film was annealed and etched in CHF_3 to remove its CVD oxide cap, before the CCl_4 etch. Both samples were given a 10% overetch. The resist mask remains to demonstrate anisotropy.

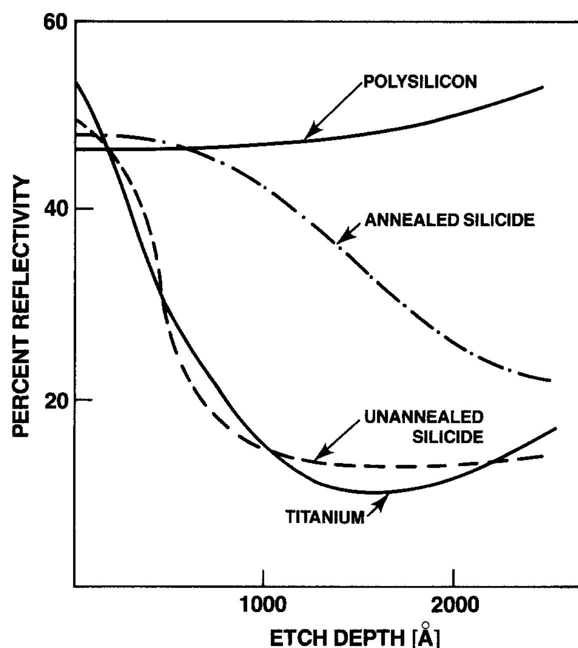

Fig. 3. Reflectivity as a function of etch depth for the CCl_4 plasma etch. The silicide films were 2 kÅ titanium silicide/2 kÅ polysilicon. The polysilicon and pure titanium films were 4 kÅ and deposited directly on 1 kÅ gate oxide.

Downloaded on 2016-02-18 to IP 130.203.136.75 address. Redistribution subject to ECS terms of use (see ecsdl.org/site/terms_use) unless CC License in place (see abstract).

GF Exhibit 1053 - 3/6

ide removal, however, bulk oxides as well as surface oxides contribute.

The use of lower selectivity etches (those with higher oxide etch rates) to eliminate the rough etching and etch residues is expanded below. Both ion milling, with silicon-to-oxide selectivities on the order of 1/1, and CF_4 reactive ion etching, where the selectivity was even less than 1/1, are considered.

Ion milling.—Argon ion milling was investigated as a function of the incidence angle as it was varied from 0° to 15°. Within experimental error, the etch rates of titanium silicide, silicon dioxide, and positive resist did not vary with angle in this range and were 170, 200, and 125 Å/min, respectively. In addition, the silicide rate did not depend on whether the film was annealed prior to etch.

The low selectivity ion milling produced much smoother etching than with CCl_4, as evidenced by a comparison of Fig. 3 and 4. Unlike the CCl_4 etch, however, annealed silicides etched more roughly then unannealed silicides. This rougher etching was attributed to the already rougher surface of the annealed silicide before etch. The well-known milling rate dependence on angle (10) would cause a rough surface to further roughen as etching proceeds.

Trenching and shadowing during the milling of actual titanium silicide features prohibited its successful use, despite its much smoother etching in open areas. A 0° incidence angle produced severe trenching along etched features. As the angle was raised from 0° to 15°, the severity of the trenching decreased, with trenching only present around isolated features at 15°. Shadowing, or slower etching between closely spaced features, however, appeared with increasing intensity as the angle was increased from 5° to 15°. Thus samples milled at 15° showed both shadowing and trenching depending on the geometry/pitch of the etching features. In short, an optimum set of conditions, one where neither trenching nor shadowing occurred, could not be found.

CF_4 etching.—Reactive ion etching with fluorine containing gases was also studied as a means of reducing the silicon-to-oxide selectivity in order to produce smooth etching of titanium containing films. Both CHF_3 and CF_4 plasmas were characterized, but since the trends/results of each were similar, only the CF_4 data will be discussed here.

Table II lists the etch rates, surface smoothness during etch, and the anisotropy obtained when utilizing a CF_4 reactant in the diode-configured reactor. The silicide etched at the same rate as polysilicon but faster than pure titanium. In addition, both thermal oxide and positive photoresist etched faster than titanium silicide and polysilicon, limiting any practical application.

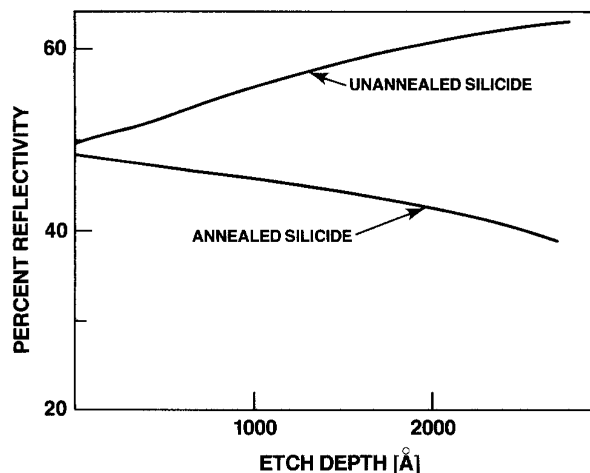

Fig. 4. Reflectivity as a function of etch depth for argon ion milling of 2 kÅ titanium silicide/2 kÅ polysilicon. The reflectivity was independent of milling angle, within the 0°-15° range studied.

Table II. CF_4 etch data from the laboratory-scale diode reactor with 7 sccm CF_4, 100 μm pressure and 0.55 W/cm^2

Film	Etch rate (Å/min)	Etch texture	Anisotropy* (with resist mask)
Titanium silicide			
Unannealed	120	Smooth	Excellent
Annealed	130	Rough	Excellent
Polysilicon	125	Smooth	Good-Fair
Titanium	60	Smooth	Excellent
Thermal SiO_2	445	—	—
Positive resist	250	—	—

* See Table I for anisotropy definitions.

The anisotropy of titanium containing films etched in CF_4 was excellent. No undercutting was ever seen for titanium silicide, while polysilicon films were undercut somewhat during extended overetches. This lower reactivity of titanium films in CF_4 is attributed to the low volatility of the expected product, TiF_4. No vapor pressure data is available on TiF_4, as it is reported in the literature simply as a white solid having a density of 2.8 g/ml which sublimes at 284°C (11).

This low volatility is, however, evidenced by the strong temperature dependence of the CF_4 etch rate of titanium silicide. Figure 5 shows data collected in the single-wafer CF_4 plasma etch. No measurable etching occurred with the wafer clamped to a 5°C electrode, while the etch rate increased from 950 to 1350 Å/min as the temperature was increased from 25° to 60°C.

The reflectivity as a function of etch depth for CF_4 etching in the diode-configured reactor is shown in Fig. 6. The unannealed silicide and pure titanium films etched very smoothly, as evidenced by the flat reflectivity. The annealed silicide, however, etched quite roughly. This trend is similar to, although more dramatic than, that observed for ion milling (see Fig. 4). The reason for the rough etching after annealing is not clear, but may be simply that, as for ion milling, the rougher surface on annealed films "facets" during etching due to an angle dependence of the etch rate.

Figure 7 compares the surface roughness of partially etched annealed and unannealed polycide samples. In addition to the obvious differences in surface texture, the SEM inspection showed no undercutting of the silicide or any problems such as trenching or shadowing.

The reverse selectivity of the fluorine-based processes makes them unsuitable for complete etching of a polycide structure. Calculations show that polysilicon-to-oxide selectivities of a least 10/1 are needed for successful etching over thin (150Å) gate oxide. Etches with selectivities that high, however, produced rough etching of oxygen containing $TiSi_2$. The solution is a two-step etch. The first step requires a low selectivity to oxide to etch

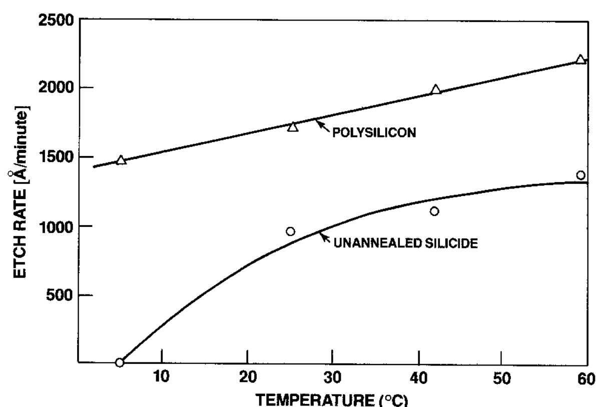

Fig. 5. The titanium silicide and polysilicon etch rates as a function of temperature in the Perkin-Elmer Cornerstone CF_4 etch process.

Downloaded on 2016-02-18 to IP 130.203.136.75 address. Redistribution subject to ECS terms of use (see ecsdl.org/site/terms_use) unless CC License in place (see abstract).

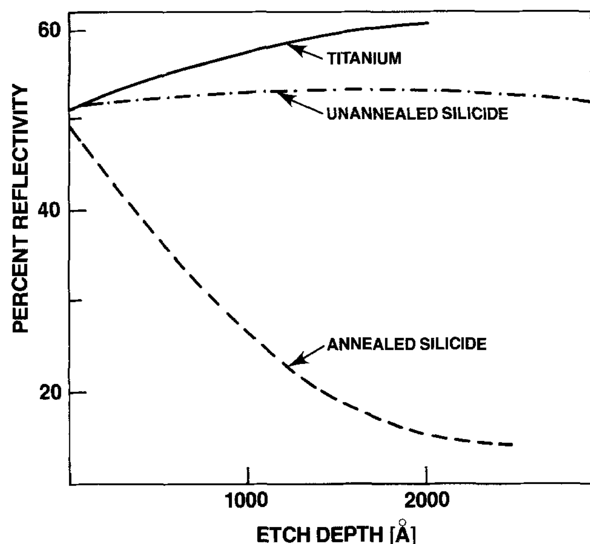

Fig. 6. Reflectivity as a function of etch depth for CF_4 reactive ion etching. The silicide films were 2 kÅ titanium silicide/2 kÅ polysilicon. The titanium film was 4 kÅ and deposited directly on gate oxide.

smoothly through the silicide, the second a high selectivity to oxide to stop at the thin underlying gate oxide.

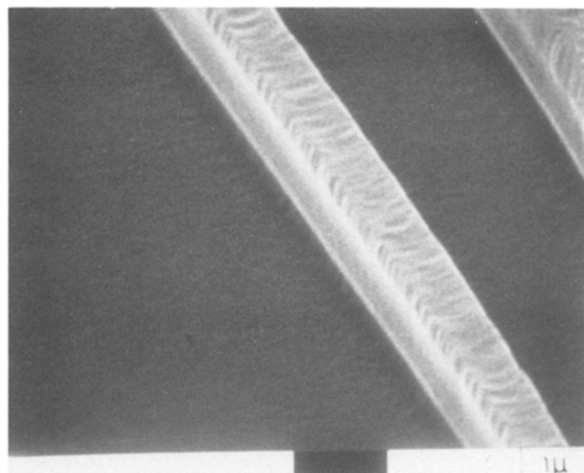

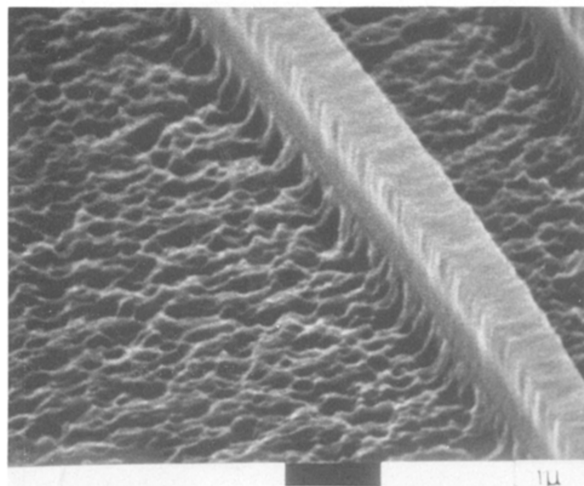

Fig. 7. Composite 2 kÅ titanium silicide/2 kÅ polysilicon films partially etched (stopped in the poly layer) in CF_4 in the laboratory scale diode reactor. The bottom film was annealed before etch. The photoresist remains on both samples.

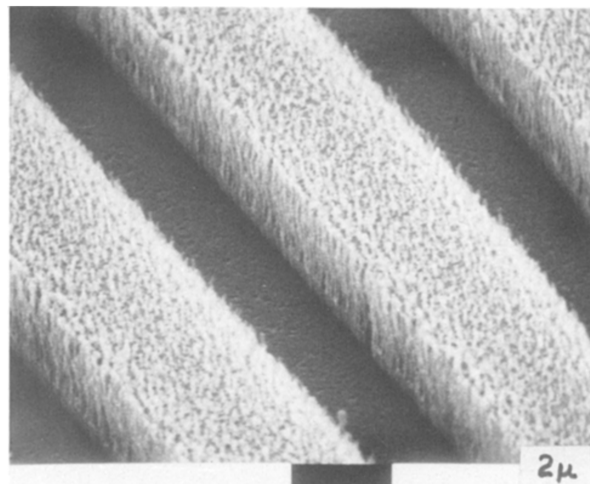

Fig. 8. Unannealed 2 kÅ titanium silicide/2 kÅ polysilicon film etched via a two-step process. Step one utilized a CF_4 reactive ion etch through the silicide. Step two was a Cl_2 plasma polysilicon etch. The photoresist remains to demonstrate anisotropy.

Two-step etching.—This section details a specific two-step etch of unannealed titanium polycides. The first step was a CF_4 reactive ion etch through the silicide, stopping in the polysilicon. The second step was a low frequency Cl_2 plasma etch of the underlying polysilicon. Figure 8 shows a sample etched via this process. Anisotropic etching with very little etch residue resulted.

The two-step etch, however, also had drawbacks. The first was simply that it was a two-step two-reactor process. A successful one-step process would certainly be more desirable. The second was that the etch selectivity with respect to photoresist was extremely poor, owing to the CF_4 etch, where resist was removed at more than twice the rate of the silicide. Trilevel resist processing (7, 8) was utilized, however, to produce the very thick submicron-sized resist patterns needed to mask this two-step process. In this manner, titanium polycide gates as small as 0.5 μm have been produced.

Certainly other two-step etch processes should work equally well. Chlorine-based plasmas produced smooth etching of oxygen containing $TiSi_2$ when the silicon-to-oxide selectivity was reduced to less than 2/1. Higher power densities, lower pressures, and hydrogen addition were combined to produce the low selectivity needed for the first step in a two-step, one-reactor etch. In addition, the resist-removal rate in the "all-chlorine" etch was substantially less than with CF_4.

Conclusions

Successful anisotropic etching of oxygen containing titanium silicide/polysilicon films could not be achieved in conventional one-step plasma etches. Selective, anisotropic chlorine-based plasmas produced unacceptably rough etching of the titanium silicide, presumably because "oxide" micromasks in/on the silicide block etching of the underlying material. Although the low selectivity of either CF_4 reactive ion etching or ion milling enabled smooth etching of unannealed silicide, the inability to stop on underlying gate oxide limited any practical application. A two-step etch, utilizing a low selectivity etch to smoothly "mill" through the silicide, followed by a high selectivity etch of the polysilicon down to the thin gate oxide, produced residue-free anisotropic etching of oxygen containing titanium polycide films.

Acknowledgments

The author wishes to thank Dr. Clarence Tracy for his helpful comments and suggestions during the etch evaluations, and for his review of this paper. Also, the film deposition and analysis performed by Carl Aspin and

Downloaded on 2016-02-18 to IP 130.203.136.75 address. Redistribution subject to ECS terms of use (see ecsdl.org/site/terms_use) unless CC License in place (see abstract).

Jerry Adams, and Auger analysis by Mike Kottke were greatly appreciated.

Manuscript submitted April 11, 1984; revised manuscript received Aug. 6, 1984.

Motorola, Incorporated, assisted in meeting the publication costs of this article.

REFERENCES

1. R. H. Dennard, F. H. Gaensslen, H. Yu, V. L. Rideout, E. Bassous, and A. R. LeBlanc, *IEEE J. Solid State Circuits*, **sc-9**, 256 (1976).
2. J. D. Meindl, K. N. Ratnakumar, L. Gerzberg, and K. C. Saraswat, in "IEEE International Solid State Circuits Conference, Digest of Technical Papers," L. Winner, Editor, p. 36, IEEE, New York (1981).
3. S. P. Murarka, *J. Vac. Sci. Technol.*, **17**, 769 (1980).
4. L. Mohammadi, *Solid State Technol.*, **1**, 65 (1981).
5. C. Aspin, Unpublished data.
6. K. L. Wang, T. C. Holloway, R. F. Pinizzotto, Z. P. Sobczak, W. R. Hunter, and A. F. Tasch, *IEEE Trans. Electron Devices*, **ed-29**, 547 (1982).
7. J. M. Moran and D. Maydan, *Bell Syst. Tech. J.*, **58**, 1027 (1979).
8. D. Maydan, *J. Vac. Sci. Technol.*, **17**, 1164 (1980).
9. "Handbook of Chemistry and Physics," 50th ed., W. C. Weast, Editor, pp. D-143, D-144, The Chemical Rubber Co., Cleveland, OH (1969).
10. S. Somekh, *J. Vac. Sci. Technol.*, **13**, 1003 (1976).
11. "Encyclopedia of Chemical Technology," 2nd ed., Vol. 20, p. 388, Interscience, New York (1967).

Thermal Diffusion Effects in Chemical Vapor Deposition Reactors

Joel P. Jenkinson and Richard Pollard*

Department of Chemical Engineering, University of Houston, Houston, Texas 77004

ABSTRACT

A mathematical model that describes the behavior of chemical vapor deposition reactors with well-defined hydrodynamics has been extended to include the effects of multicomponent thermal diffusion. The influence of thermal diffusion on the deposition rate is dependent on the deposition system and on the operating conditions of the reactor. For production of silicon by reduction of silicon tetrachloride in excess hydrogen, deposition rates are typically lowered by 15-20%. However, for deposition of boron from boron trichloride and hydrogen, thermal diffusion can raise growth rates by approximately 7% when concentrated inlet gas mixtures are used.

Chemical vapor deposition (CVD) processes are widely used in the manufacture of electronic materials and in the formation of surface coatings. Several theoretical descriptions of CVD systems have been proposed (1-15). However, the complex nature of the coupled multicomponent transport phenomena and reaction kinetics has necessitated the incorporation of many assumptions into these models. As a result, the physical factors that control the behavior of CVD reactors are only partially understood. In particular, the role and relative importance of thermal diffusion in CVD processes is a subject of controversy. Some workers feel that it can be neglected (12), whereas others state that it needs to be considered because temperature gradients are large and because there are substantial differences in the molecular weights of the reactants (13). An approximate model based on constant binary thermal diffusion ratios indicates that deposition rates could be altered significantly (15, 16). However, an order of magnitude analysis suggests that the opposite is true (12). A detailed investigation is needed to clarify the specific effects of thermal diffusion on the behavior of CVD processes.

In this paper, a previous analysis (10, 15) of CVD reactors is extended to include multicomponent thermal diffusion. Comparisons of simulations with and without thermal diffusion terms in the heat and mass transport equations are used to illustrate the effects of thermal diffusion on the performance of CVD reactors. Quantitative results are obtained for two representative CVD systems: deposition of silicon at a rotating disk, using $SiCl_4$ in excess hydrogen (17); and deposition of boron from BCl_3 and hydrogen, using an impinging jet apparatus (18).

Analysis

A steady-state model for CVD systems with an arbitrary number of chemical species has been developed previously (10, 15). The analysis includes multicomponent transport phenomena, variable physical properties, finite interfacial velocity, and simultaneous homogeneous and heterogeneous reactions. The governing equations are summarized in Table I. For laminar flow in geometries such as the rotating disk or impinging jet, Eq. [5] and [6] can be transformed into a set of ordinary differential equations, and the problem becomes one-dimensional. Also, at atmospheric pressure, it is reasonable to neglect pressure variations across the diffusion layer (10) and, hence, to use only two Navier-Stokes relations (Eq. [5]). Boundary conditions for the velocity components v_r and v_θ are dependent on the flow system (10, 15). However, the axial velocity v_z at the substrate surface is determined by the heterogeneous reaction rates, as indicated by Eq. [11]. Surface compositions are obtained with Eq. [1] and [3]. Far from the substrate, the inlet gas is assumed to be at equilibrium at the inlet gas temperature.

When thermal diffusion is included in the analysis, the multicomponent diffusion equation for an isobaric system becomes (19)

$$c_i \nabla \mu_i = RT \sum_{k \neq i} \frac{c_i c_k}{c_T \mathfrak{D}_{ik}} \left[\underline{v}_k - \underline{v}_i + \left(\frac{D_k^T}{\rho_k} - \frac{D_i^T}{\rho_i} \right) \nabla \ln T \right] \quad [12]$$

The last term on the right-hand side of Eq. [12] represents the contribution of the temperature gradient to mass transport. The method for calculating values of the multicomponent thermal diffusion coefficients D_i^T is given in the Appendix. If gas behavior is ideal, Eq. [12] may be rewritten in dimensionless form as

$$\nabla x_i - k_i^T \nabla \ln T = \sum_{k \neq i} \frac{(x_i J_k - x_k J_i)}{D_{ik}} \quad [13]$$

where D_{ik} is a dimensionless diffusion coefficient for binary interactions defined by

$$D_{ik} = c_T \mathfrak{D}_{ik} / c_\infty \nu_\infty \quad [14]$$

and k_i^T is a dimensionless multicomponent thermal diffusion ratio given by

$$k_i^T = \sum_{k \neq i} \frac{(x_i M_i D_k^T - x_k M_k D_i^T)}{M_i M_k c_\infty \nu_\infty D_{ik}} \quad [15]$$

*Electrochemical Society Active Member.

Downloaded on 2016-02-18 to IP 130.203.136.75 address. Redistribution subject to ECS terms of use (see ecsdl.org/site/terms_use) unless CC License in place (see abstract).

GF Exhibit 1053 - 6/6